Applied Physics Letters

RESEARCH ARTICLE | JANUARY 13 2025

Growth and characterization of high-quality Zr doped AlN epilayers

H. Alwan ; N. K. Hossain ; J. Li ; J. Y. Lin ; H. X. Jiang

Check for updates

Appl. Phys. Lett. 126, 022106 (2025)
https://doi.org/10.1063/5.0250015

View Online
Export Citation

Articles You May Be Interested In

Transforming underground to surface mining operation – A geotechnical perspective from case study

AIP Conference Proceedings (November 2021)

Monthly prediction of rainfall in nickel mine area with artificial neural network

AIP Conference Proceedings (November 2021)

Estimation of Karts groundwater based on geophysical methods in the Monggol Village, Saptosari District, Gunungkidul Regency

AIP Conference Proceedings (November 2021)

13 January 2025 17:45:53

AIP Publishing

Applied Physics Letters

Special Topics Open for Submissions

Learn More

AIP Publishing

Applied Physics Letters ARTICLE pubs.aip.org/aip/apl

Growth and characterization of high-quality Zr doped AlN epilayers

Cite as: Appl. Phys. Lett. **126**, 022106 (2025); doi: 10.1063/5.0250015
Submitted: 21 November 2024 · Accepted: 30 December 2024 ·
Published Online: 13 January 2025

View Online Export Citation CrossMark

H. Alwan, N. K. Hossain, J. Li, J. Y. Lin, and H. X. Jiang[a)]

AFFILIATIONS

Department of Electrical and Computer Engineering, Texas Tech University, Lubbock, Texas 79409, USA

[a)]Author to whom correspondence should be addressed: hx.jiang@ttu.edu

ABSTRACT

AlN stands out for its remarkable figures of merit for electronic and photonic devices, attributed to its ultrawide bandgap of ∼6.1 eV and an exceptionally high critical field of ∼15 MV/cm. More recently, zirconium (Zr) doped AlN (AlN:Zr) has also been identified as a promising material platform for the exploration of solid-state qubits for quantum information and technology, high performance piezoelectric acoustic wave resonators, and optically triggered ultrafast power switching devices facilitated by optically activating Zr related impurities. Despite the significant potential, the ability for producing AlN:Zr epitaxial structures has yet to be established. In this study, we have achieved AlN:Zr epilayers with a high Zr doping level $[N_{Zr}]$ of up to 10^{20} cm^{-3} using industrial standard metal-organic chemical vapor deposition growth technique. High crystalline quality of AlN:Zr was confirmed by x-ray diffraction, revealing a narrow full width at half maximum of the (002) rocking curve at 216 arcsec for 1.8 μm thick epilayers deposited on sapphire at $[N_{Zr}]=10^{20}$ cm^{-3}. Zr doping was observed to slightly increase the c-lattice constant to 4.992 Å for AlN:Zr (at $[N_{Zr}]=10^{20}$ cm^{-3}) compared to 4.980 Å for undoped AlN. X-ray photoelectron spectroscopy measurement results verified the substitution of Zr at the Al site (Zr_{Al}). The formation of (Zr_{Al}–V_N) complexes, which are predicted to possess all the desired properties required by quantum qubits, was confirmed through optical absorption studies. The realization of high-quality AlN:Zr epilayers significantly broadens the scope of technologically significant device applications for AlN.

Published under an exclusive license by AIP Publishing. https://doi.org/10.1063/5.0250015

13 January 2025 17:45:53

III-nitride semiconductor light emitting diodes (LEDs) and power electronic devices have revolutionized the lighting industry and power conversion systems by providing brighter and more energy efficient and more reliable lighting solutions and power electronic devices such as inverters and converters,[1–9] thereby enabling drastic reduction in energy consumption and environmental impact. The development of III-nitride microLED technology has created the microLED display industry and propelled the research field of microLED microdisplays for argument reality, virtual reality, and three-dimensional (AR/VR/3D) displays.[10–14] High In-content InGaN and Al-content AlGaN alloys based photonic devices are making inroads into full spectrum solar energy conversion, sterilization, and UV curing technologies.[15–18] Among III-nitrides, AlN possesses exceptionally high figures of merit (FOM) for electronic and photonic devices, owing to its ultrawide energy bandgap (UWBG) of ∼6.1 eV,[19] a critical field of ∼15 MV/cm,[9] electron mobility of $\mu_e > 300$ cm^2/V·s,[20] and thermal conductivity of ∼320 W/m·K.

Apart from traditional photonics and electronics applications of AlN, there have been surging interest in exploring point defects and doped impurities in AlN as room temperature quantum qubits.[21–23] This is because UWBG can suppress coupling between defect levels in the band gap and bulk states, and its small spin-orbit splitting can enhance qubit-state lifetime.[21] It is particularly intriguing that among various defects and impurities, zirconium (Zr) is shown to be one of the best qubit candidates because it can easily be incorporated into AlN and substitutes on the Al site (Zr_{Al}) with a low formation energy and tends to form complexes with nitrogen vacancy (Zr_{Al}-V_N), leading to formation of individually addressable qubits in this material. Though Zr_{Al} donors cannot be used as qubits, (Zr_{Al}-V_N) complexes have spin properties like N-V centers in diamonds and possess all the desired properties required by quantum qubits.[21] This prediction has simulated several experimental studies of exploring Zr implanted AlN thin films for quantum emitters.[22,23] Mg and Zr co-doped AlN polycrystalline films have also been explored for high performance piezoelectric acoustic wave resonator devices.[24] In these studies, Zr was introduced by ion implantation and followed by thermal annealing. It is quite encouraging that single photon emission lines in the visible wavelengths were observed in Zr implanted AlN thin films with one of which appearing around 1.7–1.8 eV, in agreement with the predicated energy level of (Zr_{Al}-V_N) complex in AlN.[22,23] There are obvious

Published under an exclusive license by AIP Publishing

disadvantages to employing ion implantation techniques to obtain Zr doped AlN, which include radiation damage to AlN films and difficulties in controlling the concentrations and positions of Zr_{Al}, V_N, and (Zr_{Al}-V_N) complex.

Because the predicted energy levels of Zr_A and (Zr_{Al}-V_N) of about 1.4 and 1.8 eV below the conduction band edge are sufficiently deep, and Zr_A and (Zr_{Al}-V_N) have a neutral charge state, Zr doped AlN epilayers (AlN:Zr) potentially enable the realization of extrinsic UWBG photoconductive semiconductor switches (PCSSs). PCSSs are a unique set of sub-class power electronic switching devices capable of providing reliable ultrafast high voltage or high current operation with negligible jitter time,[25–29] while the use of GaN and SiC wide bandgap (WBG) semiconductors can provide high operating voltage or current, but not both. This is because WBG PCSS devices need to employ semi-insulating materials, which were achieved by compensation doping using deep level acceptors.[25–29] This approach cannot accommodate high hold-off voltage and high photocurrent simultaneously because the total impurity concentration is too high to enable a high hold-off voltage, whereas the number of optically active compensated acceptors is generally too low to support a high photocurrent operation. Additionally, in compensation doped semi-insulating SiC and GaN, the electron mobilities are predominantly affected by ionized impurities, whereas the electron mobility in AlN:Zr is primarily influenced by neutral impurities. Based on the intrinsic physical properties of AlN and predicted Zr and (Zr_{Al}-V_N) donor energy levels, AlN:Zr PCSS devices have the potential to support optical trigger, high hold-off voltage, high on-state current, high frequency, and compact operation simultaneously. To realize the full potential of AlN:Zr material system as a platform for the investigation of solid-state qubits and PCSS devices, the ability for producing epitaxial layers with high crystalline quality using industrial standard growth techniques, such as metal-organic chemical vapor deposition (MOCVD), must be established.

We report on the epitaxial growth of AlN:Zr epilayers by MOCVD. To produce AlN:Zr, we employ epitaxial growth conditions established for undoped and Si doped AlN epilayers.[19,30] Trimethylaluminum (TMAl) and NH_3 were used as Al and N precursors, respectively, and hydrogen was used as the carrier gas. The metal-organic (MO) Zr doping source, Tetrakis(dimethylamino)zirconium (TDMAZr, $Zr[N(CH_3)_2]_4$), was carried into the reactor using hydrogen gas using a flow rate of 200 ml/min. The vapor pressure of the Zr doping source was controlled at 0.022 mm Hg at 300 K. AlN:Zr epilayers of 1.8 μm were deposited directly on c-plane sapphire via a 20 nm thick low temperature undoped AlN buffer layer grown at 750 °C, as schematically illustrated in Fig. 1(a). With no intermediate undoped AlN epilayer inserted in between the substrate and doped layer, this simple structure allows examination of AlN:Zr epilayer properties without complications and rapid feedback to improve growth conditions. The growth temperature for AlN:Zr epilayer was 1250 °C, providing a growth rate of around 0.9 μm/h. Secondary ion mass spectrometry (SIMS) measurements were performed (by Charles Evans & Associates) to determine the Zr doping concentration in AlN:Zr epilayers. X-ray photoelectron spectroscopy (XPS) technique (Physical Electronics PHI 5000 Versa Probe II Hybrid) was used in tandem to SIMS to characterize the elemental compositions of the epilayers, and the measurement was done in a high vacuum (10^{-7} Torr) chamber. An argon (Ar) ion gun was used to etch the surface to remove any dust and surface adsorbents prior to survey scans. The

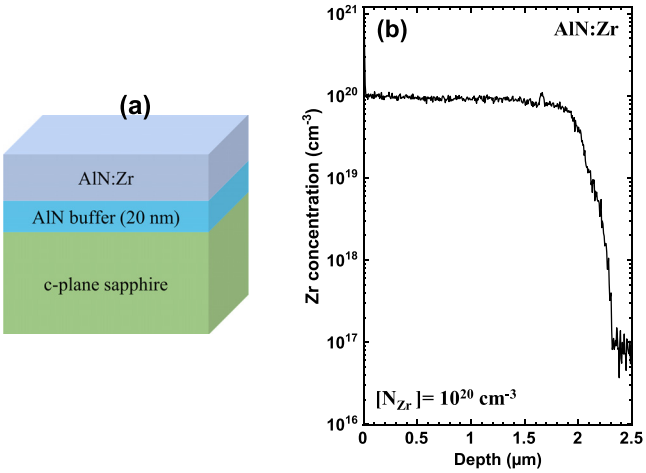

FIG. 1. (a) Schematic layer structure of AlN:Zr produced by MOCVD. (b) Plot of the Zr concentration profile measured by SIMS, revealing a uniform Zr concentration of 10^{20} cm^{-3} along the c-axis in the entire AlN:Zr epilayer.

epilayer crystalline quality was monitored by x-ray diffraction (XRD). XRD in both ω-2θ scan and ω-scan (or rocking curves) was measured to assess the effects of Zr doping to AlN:Zr crystalline quality.

Figure 1(b) plots the Zr concentration profile measured by SIMS for a representative AlN:Zr sample, revealing a uniform Zr concentration of 10^{20} cm^{-3} along the c-axis in the entire AlN:Zr epilayer. The results demonstrated that very high Zr concentrations can be attained in AlN:Zr. Based on theoretical insights, Zr dopants substitute on the Al sites and form donors (Zr_{Al}) with an energy level at ~1.4 eV below the conduction minimum. Thus, in the absence of compensating defects or impurities, Zr_{Al} donors are neutral during growth, which contrasts to the case of Si doping in AlN, in which mostly Si_{Al} donors are ionized during growth owing to a much lower ionization energy of Si_{Al} donors in AlN.

Figure 2(a) is a plot of XPS (a) survey spectrum and (b) narrow energy scan of Zr (3d) core level of an AlN:Zr epilayer. The Zr concentration estimated from the survey spectrum shown in Fig. 2(a) is around 0.3%. As XPS is a surface analysis technique (depth ~10 nm), the estimated Zr concentration from XPS not necessarily represents the precise value inside AlN:Zr, but we find a strong correlation between the Zr concentrations estimated from XPS and SIMS results. Figure 2(b) shows an XPS tight scan of the Zr ($3d_{5/2}$) core level of an AlN:Zr sample, revealing a clear peak near 180.9 eV, corresponding to Zr bonding with N (Zr-N),[31] i.e., Zr 3d with nearest neighbors of N. An additional peak near 183.3 eV is due to Zr $3d_{5/2}$–$3d_{3/2}$ orbital splitting energy of $\Delta \sim 2.4$ eV.[31] XPS results, thus, clearly demonstrated that Zr substitutes at the Al site and forms donor (Zr_{Al}) in AlN, in agreement with theoretical prediction.[21] The narrow line widths of these two peaks indicate high crystalline quality of Zr doped AlN epilayers. While not shown, tight scans of Al 2p and N 1s revealing binding energies of 73.5 and 396.6 eV, corresponding to Al bonding with nearest neighbors of N and N bonding with nearest neighbors of Al, respectively, are in good agreement with previous reported results.[32]

Figure 3(a) compares the XRD spectra in ω-2θ scans covering the (002) peaks of AlN:Zr epilayers with different Zr concentrations

13 January 2025 17:45:53

Published under an exclusive license by AIP Publishing

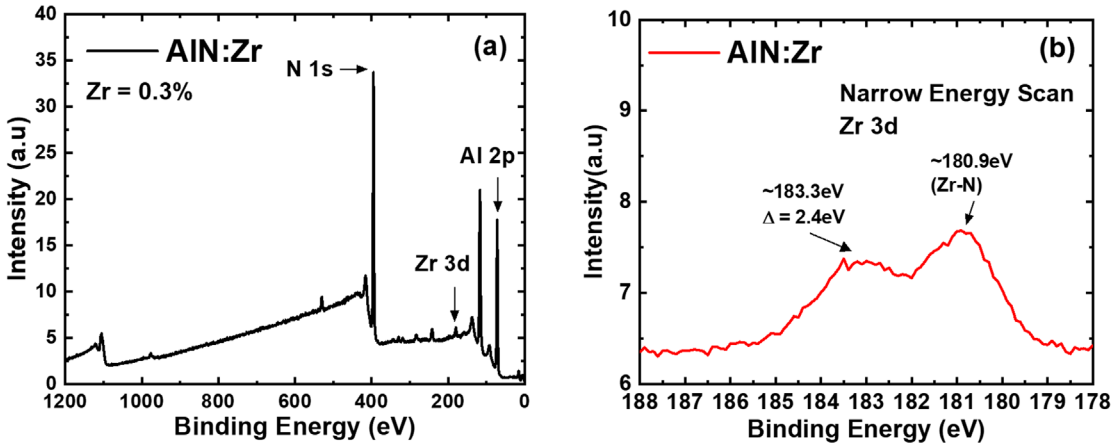

FIG. 2. (a) XPS survey spectrum performed on an AlN:Zr epilayer with a measured Zr concentration by SIMS of 10^{20} cm^{-3}. (b) XPS tight scan of Zr (3d) peaks in an AlN:Zr epilayer with a measured Zr concentration by SIMS of 10^{20} cm^{-3}.

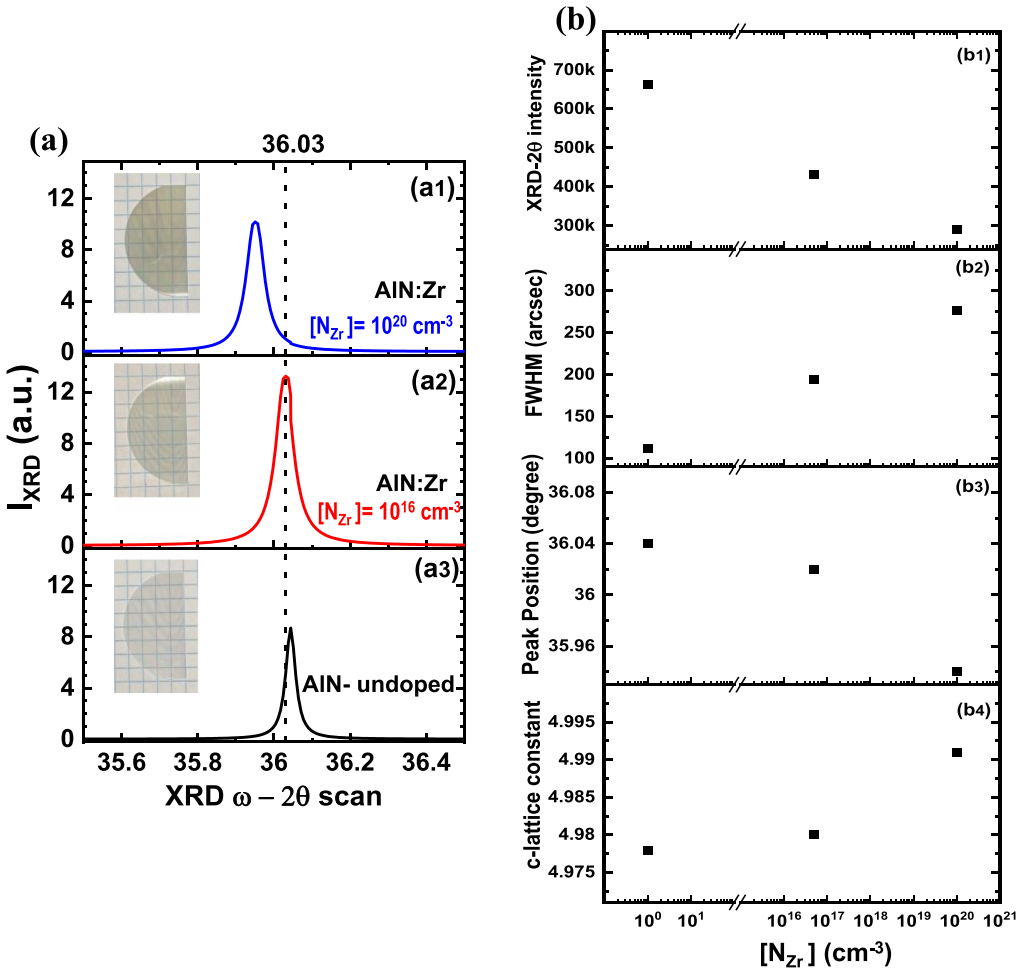

FIG. 3. (a) XRD ω-2θ scans of the (002) peaks of AlN:Zr epilayers with different Zr concentrations: (a1) $[N_{Zr}]=0$, (a2) $[N_{Zr}]=10^{16}$ cm^{-3}, and (a3) $[N_{Zr}]=10^{20}$ cm^{-3}. The dashed vertical line indicates the (002) peak in unstrained and undoped AlN. Insets are optical microscopy images of 2 in.-diameter AlN:Zr and AlN wafers. Plots of (b1) XRD intensity of (002) peak, (b2) FWHM of (002) peak, (b3) 2θ position of (002) peak, and (b4) c-lattice constant extrapolated from (002) peak position, as functions of Zr concentration.

13 January 2025 17:45:53

Published under an exclusive license by AIP Publishing

[N_{Zr}], (a1) [N_{Zr}]=0, (a2) [N_{Zr}]=10^{16} cm^{-3}, and (a3) [N_{Zr}] =10^{20} cm^{-3}, which revealed that the 2θ position of the (002) peak systematically shifted toward lower angles with increasing [N_{Zr}]. To provide a more complete picture, Fig. 3(b) plots (b1) XRD intensity of (002) peak, (b2) full width at half maximum (FWHM) of (002) peak, (b3) 2θ position of (002) peak, and (b4) c-lattice constants extrapolated from (002) peak positions, as functions of [N_{Zr}]. Several effects induced by Zr doping in AlN epilayers have been observed from Fig. 3. The XRD intensity of (002) peak in ω-2θ scans decreases, while FWHM of (002) peak in ω-2θ scans increases from 112 to 277 arcsec with increasing [N_{Zr}] from [N_{Zr}]=0 to [N_{Zr}]=10^{20} cm^{-3}. This indicates that the crystalline quality of Zr doped AlN epilayers decreases with an increase [N_{Zr}]. This can be understood by the fact that the atomic size of Zr, which substitutes on the Al site, is larger than that of Al atom. Consequently, nitrogen atoms of the nearest neighbors of Zr may be slightly distorted to compensate for strain introduced by Zr incorporation. This fact is also reflected in Figs. 3(b3) and 3(b4), which revealed that the (002) peak position shifts toward smaller angles, corresponding to an increase in the c-lattice constant with increasing Zr concentration. The c-lattice of AlN:Zr is c = 4.992 Å at [N_{Zr}] =10^{20} cm^{-3} compared to c = 4.980 Å in undoped AlN. A previous study on Mg and Zr co-doped AlN revealed a similar trend, although those AlN:MgZr polycrystalline films produced by radio-frequency magnetron reactive sputtering exhibit a FWHM of (002) peak in ω scans of 6°.[24] The incorporation of Zr also results in a slight increase in the surface roughness of the AlN epilayers. Atomic force microscopy (AFM) measurements conducted over a 5 μm × 5 μm area revealed a typical root-mean-square (RMS) surface roughness of ~1 nm for undoped AlN, compared to ~3 nm for AlN:Zr at N_{Zr}=10^{20} cm^{-3}.

Figure 4(a) compares the XRD (002) rocking curves of AlN:Zr epilayers with different Zr concentrations [N_{Zr}], (a1) [N_{Zr}]=0, (a2) [N_{Zr}]=10^{16} cm^{-3}, and (a3) [N_{Zr}]=10^{20} cm^{-3}. Figure 4(b) plots (b1) (002) XRD rocking curve intensity and (b2) (002) rocking curve FWHM as functions of Zr doping concentration, [N_{Zr}]. Several points are worth noting. First, the FWHM of (002) XRD rocking curve of our undoped AlN epilayer is as small as 20.5 arcsec, which is among the narrowest linewidth reported for AlN epilayers of this thickness. The XRD results clearly demonstrate our ability for producing AlN epilayers with the highest possible crystalline quality, which is critical to support the growth of Zr doped AlN. Second, we noted that the FWHM increases, meaning the crystalline quality of Zr doped AlN epilayers reduces with increasing [N_{Zr}], corroborating the results of Fig. 3. However, the crystalline quality of AlN:Zr remains very high even at a Zr concentration of [N_{Zr}]=10^{20} cm^{-3}, as reflected by the FWHM of (002) XRD rocking curve of only 216 arcsec for AlN:Zr with [N_{Zr}]=10^{20} cm^{-3}. In comparison, the FWHM of (002) XRD rocking curves of Zr implanted and thermally annealed AlN:Zr films produced by reactive magnetron sputtering technique exhibited a typical FWHM of greater than 1.3°.[22] In fact, the FWHM of our AlN:Zr epilayers produced by MOCVD is comparable to those seen in

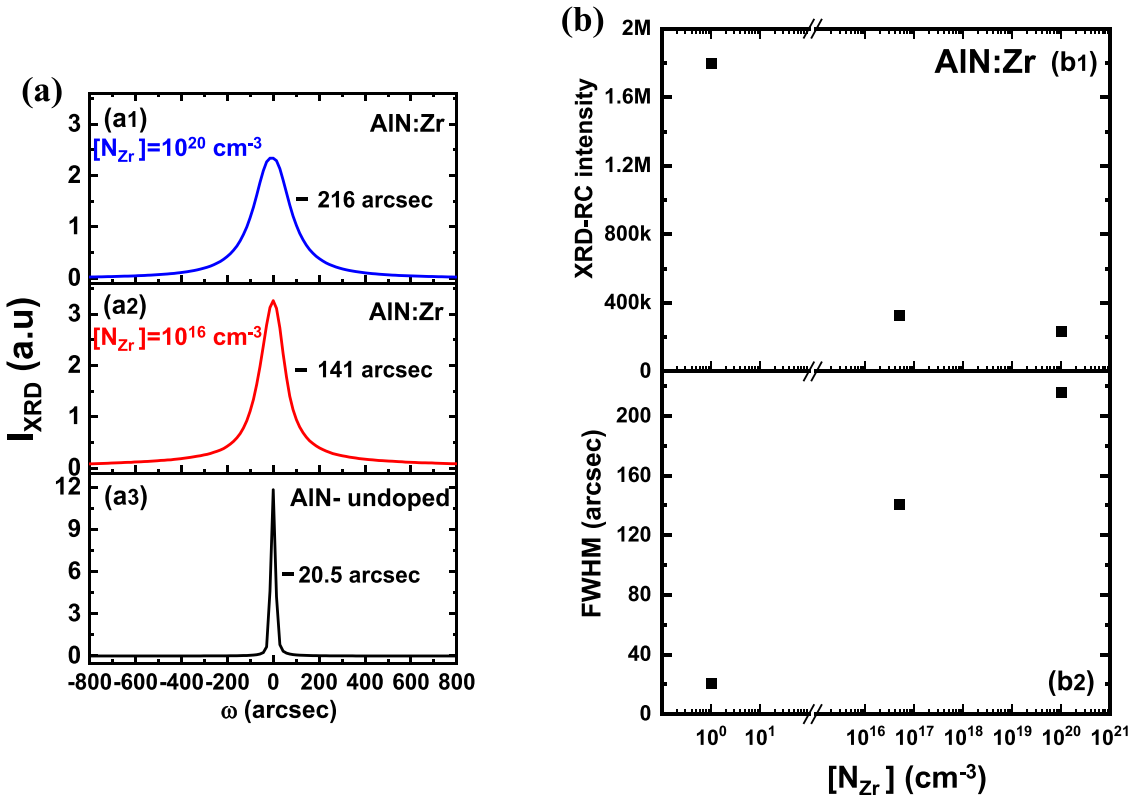

FIG. 4. (a) XRD (002) rocking curves of AlN:Zr epilayers with different Zr concentrations, (a1) [N_{Zr}]=0, (a2) [N_{Zr}]=10^{16} cm^{-3}, and (a3) [N_{Zr}]=10^{20} cm^{-3}. (b) Plots of (b1) (002) XRD rocking curve (XRD-RC) intensity and (b2) (002) rocking curve FWHM as functions of Zr doping concentration, [N_{Zr}].

13 January 2025 17:45:53

Published under an exclusive license by AIP Publishing

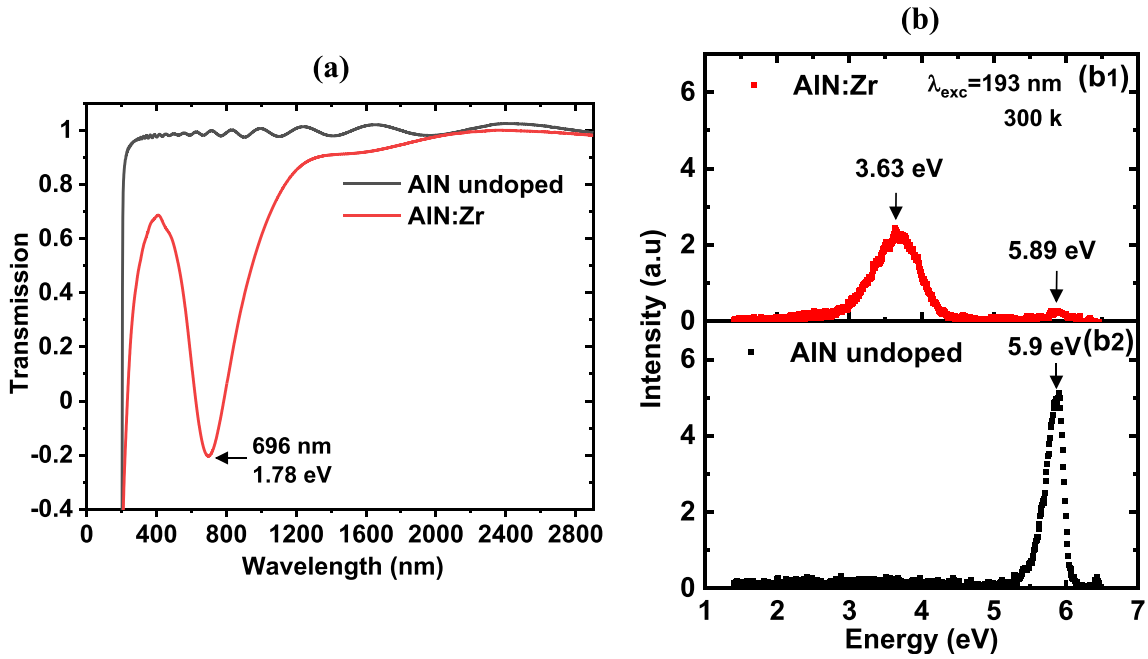

FIG. 5. Comparison of optical properties of undoped AlN and AlN:Zr ($[N_{Zr}]=10^{20}\,cm^{-3}$). (a) Room temperature optical transmission spectra of undoped AlN and AlN:Zr epilayers. (b) Room temperature PL emission spectra of undoped AlN and AlN:Zr epilayers under excitation by 193 nm photons provided by an excimer laser.

undoped AlN bulk crystals produced by the physical vapor transport method by various groups.[33,34]

Figure 5(a) compares room temperature optical transmission spectra of undoped AlN and AlN:Zr epilayers. Undoped AlN epilayer exhibits a sharp absorption at the band-edge near 200 nm, as expected from AlN with high crystalline quality and purity. In comparison, in addition to the strong optical absorption at the band-edge, AlN:Zr epilayer also exhibits a strong absorption peak at 1.78 eV. This absorption peak coincides exceptionally well with the calculated energy level of $(Zr_{Al}\text{-}V_N)^0$ donor of about 1.8 eV below the conduction band minimum in AlN:Zr, which was predicted to possess all the desired properties of quantum qubits.[21] However, the optical absorption spectrum is unable to resolve the energy level of the predicated simple substructional $(Zr_{Al})^0$ donor. Figure 5(b) compares room temperature photoluminescent (PL) emission spectra of undoped AlN and AlN:Zr epilayers under excitation by 193 nm photons provided by an excimer laser. Undoped AlN epilayer exhibits a very clean band edge emission line at 5.9 eV, whereas the dominant emission of AlN:Zr appears at around 3.63 eV with the band-edge line exhibiting a much smaller intensity as well as a slight redshift to 5.89 eV. The 3.63 eV line has not been previously observed in AlN[19,35] and is presumably related to Zr incorporation. Detailed PL emission studies are urgently needed and become possible with the realization of high-quality AlN:Zr epilayers.

In summary, we have conducted MOCVD growth of Zr doped AlN epilayers (AlN:Zr) on c-plane sapphire using MOCVD. By first establishing the capability for producing exceptionally high crystalline quality undoped AlN epilayers exhibiting a FWHM of (002) XRD rocking curve as low as 20 arcsec, AlN:Zr with a Zr concentration up to $[N_{Zr}]=10^{20}\,cm^{-3}$ has been produced. The incorporation of Zr was confirmed through a variety of characterization techniques, including SIMS, XPS, XRD, optical absorption, and PL measurements. The high crystalline quality of AlN:Zr was evidenced by a very narrow FWHM of 216 arcsec for the (002) XRD rocking curve at $[N_{Zr}]=10^{20}\,cm^{-3}$, which is significantly lower than the FWHM values of greater than degrees previously reported for AlN:Zr thin films produced using other techniques. It was observed that the c-lattice constant of AlN:Zr (4.992 Å at $N_{Zr}=10^{20}\,cm^{-3}$) is slightly enlarged over that of undoped AlN epilayer of the same thickness (4.980 Å) due to the fact that Zr substitutes at the Al site, as Zr has a larger atomic size than Al. The formation of $(Zr_{Al}\text{-}V_N)$ complexes, which are predicted to possess the desired properties for quantum qubit applications, was confirmed through optical absorption spectroscopy. Our results demonstrated that MOCVD is an ideal technique for producing AlN:Zr epitaxial films and nanostructures. The realization of AlN:Zr epilayers with excellent crystalline quality paves the way for exploring numerous advanced applications predicted by theoretical studies, including single photon emitters and solid-state qubits in AlN:Zr for quantum information and technology, improved acoustic wave resonator devices, and UWBG PCSS devices via optical activation of $(Zr_A)^0$ and $(Zr_{Al}\text{-}V_N)^0$ donors, thereby further expanding the applications of III-nitride semiconductors.

The information, data, or work presented herein was funded in part by the Advanced Research Projects Agency-Energy (ARPA-E), U.S. Department of Energy, under ULTRAFAST program, Award Number DE-AR0001821, monitored by Dr. Olga Spahn and Dr. Eric Carlson. The views and opinions of authors expressed herein do not necessarily state or reflect those of the United States Government or any agency thereof. J. Y. Lin and H. X. Jiang are grateful to the AT&T Foundation for the support of Ed Whitacre and Linda Whitacre endowed chairs.

13 January 2025 17:45:53

Published under an exclusive license by AIP Publishing

AUTHOR DECLARATIONS

Conflict of Interest

The authors have no conflicts to disclose.

Author Contributions

H. Alwan: Data curation (equal); Formal analysis (equal); Investigation (equal); Methodology (equal); Software (equal); Validation (equal); Visualization (equal). **N. K. Hossain:** Data curation (equal); Formal analysis (equal); Investigation (equal); Methodology (equal); Software (equal); Validation (equal); Visualization (equal). **J. Li:** Data curation (equal); Formal analysis (equal); Investigation (equal); Methodology (equal); Project administration (equal); Resources (equal); Software (equal); Supervision (equal); Validation (equal); Visualization (equal). **J. Y. Lin:** Conceptualization (equal); Formal analysis (equal); Funding acquisition (equal); Investigation (equal); Methodology (equal); Project administration (equal); Resources (equal); Supervision (equal); Validation (equal); Visualization (equal); Writing – original draft (equal); Writing – review & editing (equal). **H. X. Jiang:** Conceptualization (equal); Formal analysis (equal); Funding acquisition (equal); Investigation (equal); Methodology (equal); Project administration (equal); Resources (equal); Supervision (equal); Validation (equal); Visualization (equal); Writing – original draft (equal); Writing – review & editing (equal).

DATA AVAILABILITY

The data that support the findings of this study are available within the article.

REFERENCES

[1] S. Pimputkar, J. S. Speck, S. P. DenBaars, and S. Nakamura, "Prospects for LED lighting," Nat. Photonics **3**, 180 (2009).
[2] H. Amano, N. Sawaki, I. Akasaki, and Y. Toyoda, "Metalorganic vapor phase epitaxial growth of a high quality GaN film using an AlN buffer layer," Appl. Phys. Lett. **48**, 353 (1986).
[3] S. Nakamura, T. Mukai, and M. Senoh, "Candela-class high-brightness InGaN/AlGaN double-heterostructure blue-light-emitting diodes," Appl. Phys. Lett. **64**, 1687 (1994).
[4] M. A. Khan, R. A. Skogman, R. G. Schulze, and M. Gershenzon, "Electrical properties and ion implantation of epitaxial GaN, grown by low pressure metalorganic chemical vapor deposition," Appl. Phys. Lett. **42**, 430 (1983).
[5] M. Asif Khan, A. Bhattarai, J. N. Kuznia, and D. T. Olson, "High electron mobility transistor based on GaN-AlxGa1-xN heterojunction," Appl. Phys. Lett. **63**, 1214 (1993).
[6] H. Amano, Y. Baines, E. Beam *et al.*, "The 2018 GaN power electronics roadmap," J. Phys. D: Appl. Phys. **51**, 163001 (2018).
[7] I. C. Kizilyalli, O. B. Spahn, and E. P. Carlson, "Recent progress in wide-bandgap semiconductor devices for a more electric future," ECS Trans. **109**, 3 (2022).
[8] Y. H. Chen, J. Encomendero, C. Savant, V. Protasenko, H. G. Xing, and D. Jena, "Electron mobility enhancement by electric field engineering of AlN/GaN/AlN quantum-well HEMTs on single-crystal AlN substrates," Appl. Phys. Lett. **124**, 152111 (2024).
[9] T. L. Chu and R. W. Kelm, "The preparation and properties of aluminum nitride films," J. Electrochem. Soc. **122**, 995 (1975).
[10] S. X. Jin, J. Li, J. Z. Li, J. Y. Lin, and H. X. Jiang, "GaN microdisk light emitting diodes," Appl. Phys. Lett. **76**, 631 (2000).
[11] H. X. Jiang, S. X. Jin, J. Li, J. Shakya, and J. Y. Lin, "III-nitride blue microdisplays," Appl. Phys. Lett. **78**, 1303 (2001).
[12] J. Day, J. Li, D. Y. C. Lie, C. Bradford, J. Y. Lin, and H. X. Jiang, "III-nitride full-scale high-resolution microdisplays," Appl. Phys. Lett. **99**, 031116 (2011).
[13] H. X. Jiang and J. Y. Lin, "How we made the microLED," Nat. Electron. **6**, 257 (2023).
[14] P. J. Parbrook, B. Corbett, J. Han, T. Y. Seong, and H. Amano, "Micro-light emitting diode: From chips to applications," Laser Photonics Rev. **15**, 2000133 (2021).
[15] J. Wu, W. Walukiewicz, K. Yu, J. W. Ager III, E. E. Haller, H. Lu, W. J. Schaff, Y. Saito, and Y. Nanishi, "Small band gap bowing in InGaN alloys," Appl. Phys. Lett. **80**, 4741 (2002).
[16] S. Vanka, B. Zhou, R. A. Awni, Z. Song, F. A. Chowdhury, X. Liu, H. Hajibabaei, W. Shi, Y. Xiao, I. A. Navid, A. Pandey, R. Chen, G. A. Botton, T. W. Hamann, D. Wang, Y. Yan, and Z. Mi, "InGaN/Si double-junction photocathode for unassisted solar water splitting," ACS Energy Lett. **5**, 3741 (2020).
[17] M. A. Khan, K. Balakrishnan, and T. Katona, "Ultraviolet light-emitting diodes based on group three nitrides," Nat. Photonics **2**, 77 (2008).
[18] Z. Zhang, M. Kushimoto, T. Sakai, N. Sugiyama, L. J. Schowalter, C. Sasaoka, and H. Amano, "A 271.8 nm deep-ultraviolet laser diode for room temperature operation," Appl. Phys. Express **12**, 124003 (2019).
[19] J. Li, K. B. Nam, M. L. Nakarmi, J. Y. Lin, H. X. Jiang, P. Carrier, and S.-H. Wei, "Band structure and fundamental optical transitions in wurtzite AlN," Appl. Phys. Lett. **83**, 5163 (2003).
[20] P. Bagheri, C. Quiñones-Garcia, D. Khachariya, S. Rathkanthiwar, P. Reddy, R. Kirste, S. Mita, J. Tweedie, R. Collazo, and Z. Sitar, "High electron mobility in AlN: Si by point and extended defect management," J. Appl. Phys. **132**, 185703 (2022).
[21] J. B. Varley, A. Janotti, and C. G. Van de Walle, "Defects in AlN as candidates for solid-state qubits," Phys. Rev. B **93**, 161201(R) (2016).
[22] A. Aghdaei, R. Pandiyan, B. Ilahi, M. Chicoine, M. E. Gowini, F. Schiettekatte, L. G. Fréchette, and D. Morris, "Engineering visible light emitting point defects in Zr-implanted polycrystalline AlN films," J. Appl. Phys. **128**, 245701 (2020).
[23] A. Senichev, Z. O. Martin, Y. Wang, O. M. Matthiessen, A. Lagutchev, H. Htoon, A. Boltasseva, and V. M. Shalaev, "Quantum emitters in aluminum nitride induced by heavy ion irradiation," APL Quantum **1**, 036103 (2024).
[24] T. Yokoyama, Y. Iwazaki, Y. Onda, T. Nishihara, Y. Sasajima, and M. Ueda, "Effect of Mg and Zr co-doping on piezoelectric AlN thin films for bulk acoustic wave resonators," IEEE Trans. Ultrason. Ferroelectr. Freq. Control **61**, 1322 (2014).
[25] J. S. Sullivan, "Wide bandgap extrinsic photoconductive switches," Ph.D. thesis (Lawrence Livermore National Lab., 2012).
[26] S. E. Sampayan, P. V. Grivickas, A. M. Conway *et al.*, "Characterization of carrier behavior in photonically excited 6H silicon carbide exhibiting fast, high voltage, bulk transconductance properties," Sci. Rep. **11**, 6859 (2021).
[27] K. Zhu, S. Dogan, Y. T. Moon, J. Leach, F. Yun, D. Johnstone, H. Morkoç, G. Li, and B. Ganguly, "Effect of n^+-GaN subcontact layer on 4H-SiC high-power photoconductive switch," Appl. Phys. Lett. **86**, 261108 (2005).
[28] J. H. Leach, R. Metzger, E. Preble, and K. R. Evans, "High voltage bulk GaN-based photoconductive switches for pulsed power applications," Proc. SPIE **8625**, 86251Z (2013).
[29] E. Majda-Zdancewicz, M. Suproniuk, M. Pawłowski, and M. Wierzbowsk, "Current state of photoconductive semiconductor switch engineering," Opto-Electron. Rev. **26**, 92 (2018).
[30] M. L. Nakarmi, K. H. Kim, K. Zhu, J. Y. Lin, and H. X. Jiang, "Transport properties of highly conductive n-type Al-rich $Al_xGa_{1-x}N$ ($x \geq 0.7$)," Appl. Phys. Lett. **85**, 3769 (2004).
[31] M. Del Re, R. Gouttebaron, J.-P. Dauchot, P. Leclère, G. Terwagne, and M. Hecq, "Study of ZrN layers deposited by reactive magnetron sputtering," Surf. Coat. Technol. **174–175**, 240 (2003).
[32] L. Rosenberger, R. Baird, E. McCullen, G. Auner, and G. Shreve, "XPS analysis of aluminum nitride films deposited by plasma source molecular beam epitaxy," Surf. Interface Anal. **40**, 1254 (2008).
[33] Q. Wang, D. Lei, G. He, J. Gong, J. Huang, and J. Wu, "Characterization of 60 mm AlN single crystal wafers grown by the physical vapor transport method," Phys. Status Solidi (a) **216**, 1900118 (2019).
[34] W. H. Chen, Z. Y. Qin, X. Y. Tian, X. H. Zhong, Z. H. Sun, B. K. Li, R. S. Zheng, Y. Guo, and H. L. Wu, "The physical vapor transport method for bulk AlN crystal growth," Molecules **24**, 1562 (2019).
[35] N. Nepal, M. L. Nakarmi, J. Y. Lin, and H. X. Jiang, "Photoluminescence studies of impurity transitions in AlGaN alloys," Appl. Phys. Lett. **89**, 092107 (2006).

13 January 2025 17:45:53

Published under an exclusive license by AIP Publishing